ECS Journal of Solid State
Science and Technology

OPEN ACCESS

Editors' Choice—Precipitation of Suboxides in Silicon, their Role in Gettering of Copper Impurities and Carrier Recombination

To cite this article: G. Kissinger *et al* 2020 *ECS J. Solid State Sci. Technol.* **9** 064002

ECS Journal of Solid State Science and Technology, 2020 **9** 064002

Editors' Choice—Precipitation of Suboxides in Silicon, their Role in Gettering of Copper Impurities and Carrier Recombination

G. Kissinger,[1,*,z] D. Kot,[1] A. Huber,[2,a] R. Kretschmer,[2] T. Müller,[2] and A. Sattler[2]

[1]*IHP—Leibniz-Institut für innovative Mikroelektronik, Im Technologiepark 25, 15236 Frankfurt (Oder), Germany*
[2]*Siltronic AG, Hanns-Seidel-Platz 4, 81737 München, Germany*

This paper describes a theoretical investigation of the phase composition of oxide precipitates and the corresponding emission of self-interstitials at the minimum of the free energy and their evolution with increasing number of oxygen atoms in the precipitates. The results can explain the compositional evolution of oxide precipitates and the role of self-interstitials therein. The formation of suboxides at the edges of SiO_2 precipitates after reaching a critical size can explain several phenomena like gettering of Cu by segregation to the suboxide region and lifetime reduction by recombination of minority carriers in the suboxide. It provides an alternative explanation, based on minimized free energy, to the theory of strained and unstrained plates. A second emphasis was payed to the evolution of the morphology of oxide precipitates. Based on the comparison with results from scanning transmission electron microscopy the sequence of morphology evolution of oxide precipitates was deduced. It turned out that it is opposite to the sequence assumed until now.

 [DOI: 10.1149/2162-8777/aba0ce]

Manuscript submitted May 26, 2020; revised manuscript received June 23, 2020. Published July 6, 2020.

Investigations of the precipitation of interstitial oxygen in Czochralski (CZ) silicon have been carried out since decades. The issue is very complex involving other species like intrinsic point defects, dopants and impurities. In addition to this, the initial stages of oxygen precipitation take place on the atomic level and cannot be observed directly until now. However, advances in diagnostic methods always provide new insights into the precipitation process. Nevertheless, there are still open issues which need to be clarified. Such issues are the getter efficiency of oxide precipitates for metallic impurities and the recombination activity of oxide precipitates in relation to their composition. First, recent hypotheses and findings are summarized here.

Starting from TEM investigations of the size of oxide precipitates and comparing it with their density determined by preferential etching and the loss of interstitial oxygen (Oi) measured by FTIR, Falster et al. found a discrepancy between the total loss of Oi and the visible loss of Oi in the form of precipitates observed by transmission electron microscopy (TEM).[1] They developed a theory which distinguishes between strained oxide precipitates, which are able to getter metallic impurities, and unstrained oxide precipitates so-called "ninja" precipitates, being not able to getter metallic impurities.[1] In a recently published paper of Voronkov et al., the "ninja" precipitates were assumed to be unstrained layers of VO_2 in silicon which after reaching a critical size transform to visible precipitates.[2] The problem with this assumption is that such layers of VO_2 are not unstrained. This was already published earlier in several ab-initio studies.[3–5] The remaining question is, why the "ninja" precipitates where not found by TEM[1] although TEM allows the observation of defects down to atomic resolution. The problem is that the high resolution does not automatically mean that all these tiny defects can be easily found. At low magnification they remain undetectable. Only step by step investigation with a well-focused beam and very high magnification in addition to a sufficiently high density of defects will be crowned with success. Modern TEM methods like scanning transmission electron microscopy (STEM) are much more suitable for the investigation of very small oxide precipitates as it was demonstrated in Ref. 6.

Until now, several phenomena are explained by the conversion from so-called unstrained to strained oxide precipitates. Bothe et al. assume that unstrained oxide precipitates do not give rise to a detectable photoluminescence signal but a broad PL peak centered at ≈1600 nm is related with strained precipitates.[7] Murphy et al. carefully isolated the lifetime contribution of oxide precipitates from other lifetime contributions and they associate very high lifetimes with unstrained precipitates.[8] According to Ref. 8 recombination at strained oxide precipitates is much stronger and rather depends on their density and less on their size. A dependence of the inverse lifetime on precipitate density was found already in Ref. 9. In a later publication, Murphy et al. reported that the density of recombination centers associated with oxide precipitates more likely depends on their interface area.[10] In any of such investigations, the density of strained oxide precipitates was assumed to be the density measured after preferential etching and the density of unstrained precipitates was always determined indirectly from the residual loss of interstitial oxygen.

Tremendous progress in the investigation of the stoichiometry of oxide precipitates was made by using electron energy loss spectrometry (EELS) carried out by scanning transmission electron microscopy (STEM).[11] It was shown that the center of oxide precipitates consists of oxygen-rich SiO_x being in most cases SiO_2 surrounded by suboxide with decreasing x towards the edges. Based on these results, Vanhellemont published a shell model to explain the various scattering stoichiometry results in literature obtained by different diagnostic techniques on different kind of oxide precipitates.[12] However, it is not yet clear if oxide precipitates always possess such a suboxide shell. Kamiyama and Sueoka carried out ab initio calculations about the stability of oxygen atoms near oxide precipitates.[13] Their results suggest that a transition layer between SiO_2 and Si can be only three atomic layers thick and thick oxides with composition $x < 2$ are unstable and unable to exist. The problem is that for their ab initio calculation, as usually, α-quartz was used to represent the oxide phase. In reality, oxide precipitates consist of amorphous silicon oxide which can much more easily exist as a suboxide.

It was also discovered recently that the suboxides surrounding oxide precipitates act as gettering sinks for Cu impurities.[14] This makes the issue, if in any case oxide precipitates are surrounded by suboxide, even more important because it could become a criterion for efficient gettering. Murphy et al. reported that iron impurities segregate to oxide precipitates and thus form additional recombination centers in addition to dangling bonds.[15,16]

In this paper, we will describe a theoretical investigation of the phase composition of oxide precipitates and the corresponding emission of self-interstitials at the minimum of the free energy and

*Electrochemical Society Member.
[a]Present address: Wacker Chemie AG, 84489 Burghausen, Germany.
[z]E-mail: gkissinger@ihp-microelectronics.com

their evolution with increasing number of oxygen atoms in the precipitates. This gave us an idea about the compositional evolution of oxide precipitates and the role of self-interstitials therein. The comparison with experimental results from ourselves and from the literature allowed us to understand the important role of suboxides for internal gettering of metallic impurities and for carrier recombination at oxide precipitates being important for lifetime control. Second emphasis is payed to the evolution of the morphology of oxide precipitates. We included the morphology into the minimization of the free energy in addition to composition and self-interstitial emission. Comparison with experimental results allowed us to deduce the sequence of morphology evolution of oxide precipitates.

Modelling

Spherical oxide precipitates.—The free energy of an oxide precipitate containing n oxygen atoms can be well described by classical nucleation theory.[17] The precipitating phase is amorphous SiO_x with $x \leqslant 2$. For simplicity, the precipitates are assumed to be spherical. Precipitates are always compressively strained because the density of a certain amount of silicon atoms before being oxidized is higher than the density after oxidation. Here we assume that the strain is relieved by the ejection of β silicon self-interstitials I per precipitated oxygen atom from the precipitate/matrix interface. Accordingly, the general equilibrium reaction of oxygen precipitation can be formulated as follows:

$$P_n + \left(\frac{1}{x} + \beta\right)Si + O \leftrightarrow P_{n+1} + \beta I + \text{strain energy} \qquad [1]$$

where P_n and P_{n+1} are precipitates containing n and $n + 1$ oxygen atoms, respectively. In the course of precipitation, a supersaturation of interstitials is generated around the precipitates.

The total free energy of formation of a spherical precipitate nucleus G consisting of n oxygen atoms contains three major contributions. These are the free energy of formation of the precipitated oxide phase G_v, the free energy necessary to create the new interface of the sphere with the silicon matrix G_σ, and the elastic strain energy G_ε caused by the volume deficiency between the spherical silicon cavity and the volume of the precipitated oxide phase. A temperature dependence of the elastic moduli and of different thermal expansion are neglected here. Most classical considerations of nucleation follow this approach. Then, the total free energy of an oxide precipitate in a closed bulk region can be obtained as follows[4]:

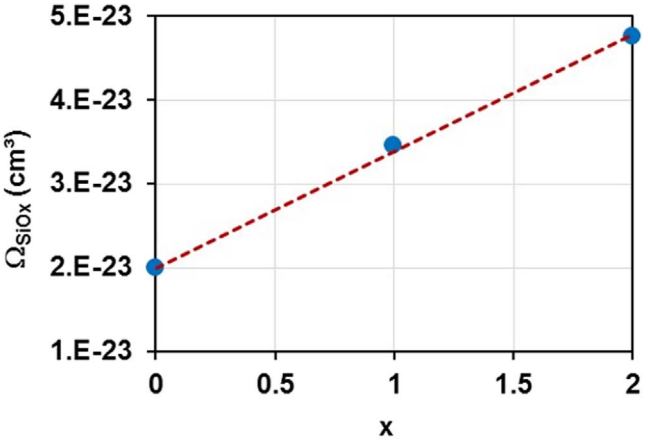

Figure 1. Molecular volume of SiO_x plotted as function of stoichiometry x of SiO_x precipitates. The molecular volume for $x = 0$ is the molecular volume of silicon and the molecular volumes of SiO and SiO_2 were taken from Refs. 17 and 20, respectively.

$$G(n, x, \beta) = -G_v + G_\sigma + G_\varepsilon \text{ with} \qquad [2]$$

$$G_v(n, x, \beta) = n \cdot k \cdot T \cdot \ln\left[\frac{(C_{Oi}^0 - n \cdot N)}{C_{Oi}^{eq}} \cdot \left(\frac{C_I^{eq}}{(C_I + F \cdot N \cdot n \cdot \beta)}\right)^{\beta}\right], \qquad [3]$$

$$G_\sigma(n, x, \beta) = (36\pi)^{\frac{1}{3}} \cdot \left(\frac{\Omega_{SiOx} \cdot n}{x}\right)^{\frac{2}{3}} \cdot \sigma \cdot \left(\frac{1+\delta}{1+\varepsilon}\right)^{-2}, \text{ and} \qquad [4]$$

$$G_\varepsilon(n, x, \beta) = \left(\frac{\Omega_{SiOx} \cdot n}{x}\right) \cdot 6 \cdot \mu \cdot \delta \cdot \varepsilon \cdot (1+\delta)^{-3}. \qquad [5]$$

Here C_I^{eq} and C_I denote the equilibrium concentration and the concentration of self-interstitials, respectively. The initial and equilibrium concentrations of interstitial oxygen are C_{Oi}^0 and C_{Oi}^{eq}, respectively. The factor F is usually set to $F = 1$ because the bulk system is regarded to be closed. It was only used to estimate the effect of out-diffusion of self-interstitials as it would be the case below the surface of a silicon wafer. For this purpose, it was varied between 1 and 0.

The strain energy according to Nabarro et al.[18] originally refers to the volume of the cavity in the matrix. Therefore, the volume misfit has to be taken into account in Eq. 5. The misfit δ and the strain ε were calculated as follows:

$$\delta = \left\{\frac{\Omega_{SiOx}}{\Omega_{Si} \cdot [1 + x\beta]}\right\}^{\frac{1}{3}} - 1 \text{ and} \qquad [6]$$

$$\varepsilon = \frac{\delta}{1 + \left(\frac{4\mu}{3K}\right)} \qquad [7]$$

with a shear modulus μ of silicon of 6.41×10^{10} Pa, a bulk modulus K of the precipitate of 3.47×10^{10} Pa, and an interface energy σ of 4.4032×10^{14} eV cm^{-2} (0.7055 J m^{-2}).

The molecular volume of silicon Ω_{Si} is 2×10^{-23} cm^3 and typical values for the molecular volumes of oxygen precipitates applied for modeling in the literature are 3.45×10^{-23} cm^3 for SiO[17] and 4.76×10^{-23} cm^3 for SiO_2.[19] These three values are plotted in Fig. 1 vs x. Because there is an obvious linear relationship, we determined the molecular volume per precipitated oxygen atom Ω_{SiOx} as a function of x by a linear fit as follows:

$$\Omega_{SiOx}(x) = 1.39 \times 10^{-23}[\text{cm}^3] \cdot x + 2 \times 10^{-23}[\text{cm}^3] \text{ for } 0 \leqslant x \leqslant 2. \qquad [8]$$

Now, we have a two-dimensional function for G and can determine for each number of precipitated oxygen atoms n the minimum of G with respect to the corresponding stoichiometry x and the interstitials to be emitted per precipitated oxygen atom β. The minimization is achieved by solving:

$$\frac{\partial G(n, x, \beta)}{\partial x} = 0 \text{ and } \frac{\partial G(n, x, \beta)}{\partial \beta} = 0 \qquad [9]$$

under the constraints $0 \leqslant x \leqslant 2$ and $0 \leqslant \beta \leqslant 0.7$. The range of β covers all possibilities from zero to full strain relief by self-interstitial emission. The value for full strain relief can be obtained by setting Eq. 6 to zero and resolving it for β. The initial concentration of interstitial oxygen C_{Oi}^0, the density of oxide precipitates N and the temperature were left constant in each simulation. The temperature affects the results via the equilibrium

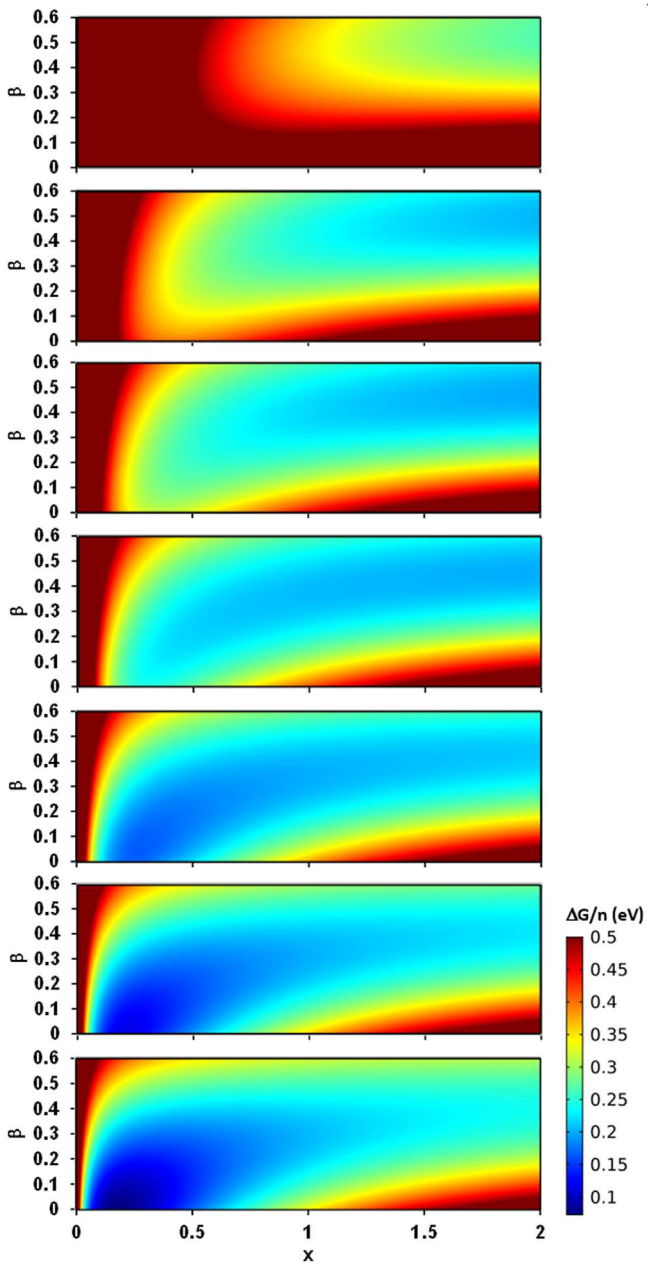

Figure 2. $\Delta G/n$ plotted as function of x and β for $n = 100$, 500, 1000, 2000, 5000, 10000, and 20000 (order from top to bottom), $N = 1 \times 10^{10}$ cm^{-3}, $C_{Oi}^{0} = 6 \times 10^{17}$ cm^{-3}, and $T = 1000$ °C.

concentrations of self-interstitials C_I^{eq} and interstitial oxygen C_{Oi}^{eq}, which were taken from Frewen et al.[20] and Mikkelsen,[21] respectively. All simulations were carried out using the software COMSOL Multiphysics.

Spheroidal oxide precipitates.—Typical morphologies of oxide precipitates are octahedrons and polyhedrons, which are first of all formed at high temperatures, and plates being typically formed during low temperature anneals (see e.g. Refs. 22–24). In modelling, the octahedrons and polyhedrons are well represented by spheres and for plate-like precipitates, oblate spheroids are a very good modeling approach.[17] Using oblate spheroids, one can also cover the full range of morphologies from plate to sphere by just varying the aspect ratio.

If we enlarge our model for oblate spheroids we have to replace the free energy necessary to create the new interface (Eq. 4) by

$$G_\sigma(n, x, \beta, \gamma) = (36\pi)^{\frac{1}{3}} \cdot \left(\frac{\Omega_{SiOx} \cdot n}{x}\right)^{\frac{2}{3}} \cdot \sigma \cdot \left(\frac{1+\delta}{1+\varepsilon}\right)^{-2} \cdot \left[\frac{1}{2} + \frac{\gamma^2}{4e} \ln\left(\frac{1+e}{1-e}\right)\right] \cdot \gamma^{-2/3} \quad [10]$$

with $e = \sqrt{1-\gamma^2}$ being the eccentricity of the ellipsoid and γ the aspect ratio. This interface free energy is valid for $0 < \gamma < 1$. For the elastic strain energy of an oblate spheroidal precipitate, Eq. 5 is replaced by

$$G_\varepsilon(n, x, \beta, \gamma) = \left(\frac{\Omega_{SiOx} \cdot n}{x}\right) \cdot 6 \cdot \mu \cdot \delta \cdot \varepsilon \cdot E(\gamma) \cdot (1+\delta)^{-3}. \quad [11]$$

Here, $E(\gamma)$ is the elastic energy of a precipitate as function of its shape according to Nabarro et al.[18]

Now, it is possible to minimize the three-dimensional function of G by solving

$$\frac{\partial G(n, x, \beta, \gamma)}{\partial \gamma} = 0, \frac{\partial G(n, x, \beta, \gamma)}{\partial x} = 0 \text{ and } \frac{\partial G(n, x, \beta, \gamma)}{\partial \beta} = 0 \quad [12]$$

under the constraints $0 < \gamma < 1$, $0 \leqslant x \leqslant 2$, and $0 \leqslant \beta \leqslant 0.7$ and to find for each n the minimum G and the corresponding aspect ratio γ, stoichiometry x, and interstitials to be emitted per precipitated oxygen atom β.

Experimental

Experimental data were generated for comparison with the results of modeling. For this purpose, Czochralski silicon wafers 200 mm in diameter, B-doped with a resistivity of about 10 Ωcm, and a concentration of interstitial oxygen $C_{Oi}^{0} = 6.5 \times 10^{17}$ cm^{-3} (conversion factor 2.45×10^{17} cm^{-2}) were used. These wafers were co-doped with 1×10^{15} cm^{-3} nitrogen. In addition to this, 150 mm Czochralski silicon wafers, B-doped with a resistivity of about 50 Ωcm, and $C_{Oi}^{0} = 8.5 \times 10^{17}$ cm^{-3} were included into the experiments. Both wafer types were pretreated by rapid thermal annealing (RTA) for 30 s at 1250 °C, 1225 °C, 1200 °C, or 1175 °C in Ar/1000 ppm O_2. Then samples were cut from the wafers and annealed at 800 °C in a conventional furnace for 1 h, 2 h, 4 h, 8 h, 16 h, or 32 h.

The density of oxide precipitates was measured by preferential etching of a (110) cleavage plane with the Secco etchant.[25] This was done after an additional growth anneal at 1000 °C for 16 h in order to grow the oxide precipitates to a size above the detection limit. Because this method allows to detect densities of bulk microdefects (BMDs) in the range from 10^7 to 10^{11} cm^{-3} it is the most suitable for our purposes. BMDs are oxide precipitates with and without secondary defects like stacking faults or dislocations. There is the danger that during the growth treatment part of the oxide precipitates cannot survive ramping because they become unstable. This is not the case for all our samples annealed at 800 °C because the BMD density measured after growth anneal remains nearly constant for all annealing times used. The density of oxide precipitates is predefined by the RTA temperature.

The getter efficiencies of the wafers with the oxide precipitates formed during annealing were measured in a Cu getter test based on time-of-flight secondary ion mass spectrometry (ToF-SIMS). This ToF-SIMS 7 day storage Cu getter test is described in detail in Ref. 26. The contamination level was in the range 4×10^{12} cm^{-2} to 1.5×10^{13} cm^{-2}. Also some of the samples with the additional growth anneal were included into the getter tests.

Morphologies of oxide precipitates in silicon wafers annealed at 1000 °C in a conventional furnace for up to 30 h were investigated

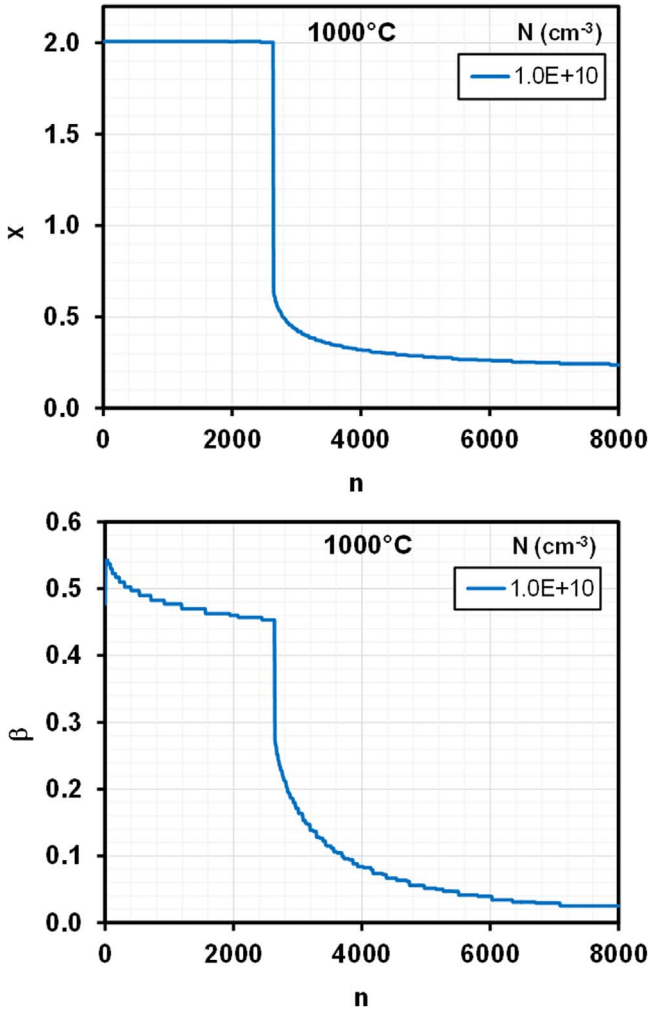

Figure 3. Both x and β plotted as function of n for $N = 1 \times 10^{10}$ cm^{-3}, $O_i = 6 \times 10^{17}$ cm^{-3}, and $T = 1000$ °C.

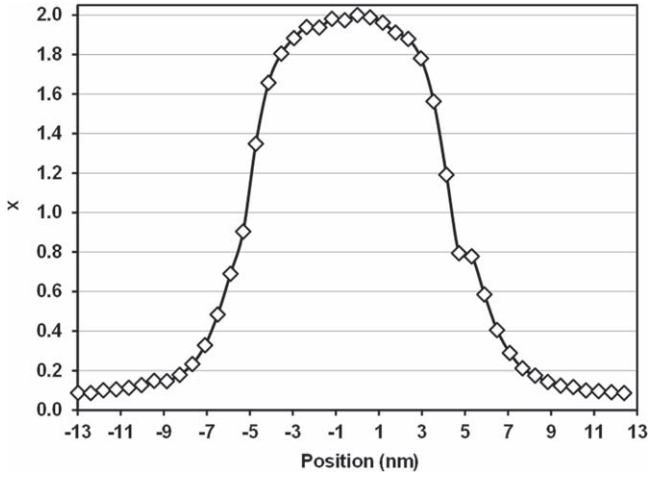

Figure 4. Stoichiometry profile across a 9.7 nm thick plate-like oxide precipitate after RTA 1250 °C 30 s followed by annealing 800 °C 8 h + 1000 °C 16 h in N_2. Reprinted from Ref. 11. Copyright 2017 with permission from the authors.

using a 200 kV scanning transmission electron microscope of FEI Tecnai Osiris equipped with a tool for energy-dispersive X-ray spectroscopy (EDX) analysis. Lamellae were prepared from the samples by grinding, polishing, and ion milling. All samples for (110) STEM lamellae were cut perpendicular to the wafer surfaces. In this way it was possible to analyze the morphology of oxide precipitates at different depths below the wafer surface.

Results of Modeling

Modeling spherical oxide precipitates.—In Fig. 2, a typical example is shown which demonstrates how β and x would behave under equilibrium conditions for different n. Here, $\Delta G/n$ is plotted as function of x and β for different n increasing from top to bottom for $N = 1 \times 10^{10}$ cm^{-3}, $O_i = 6 \times 10^{17}$ cm^{-3}, and $T = 1000$ °C. It can be seen that for low numbers of precipitating oxygen atoms the composition is SiO_2 and the self-interstitial emission relieving the strain is very high. With increasing n, the emission of self-interstitials slightly decreases until the minimum free energy suddenly jumps to low values of x and very low emission of self-interstitials. In Fig. 3, both x and β are plotted as functions of n for the same conditions as used in Fig. 2. Figure 3 demonstrates that with the increasing n, the precipitate first reduces the emission of self-interstitials up to a critical number of precipitated oxygen atoms n_{crit} before it drastically changes its stoichiometry into a suboxide.

What does this mean for the composition of oxide precipitates? Our results are related to equilibrium conditions with oxide precipitates of homogeneous composition. In reality, the growth of oxide precipitates is a dynamic process and changes in composition of already precipitated material can only occur via diffusion processes. Therefore, our modeling results suggest that in the beginning up to n_{crit} precipitates consist of SiO_2. After this point, suboxides are precipitated and a diffuse interface is formed by inter-diffusion. This is well in agreement with recently published experimental results about the stoichiometry of oxygen precipitates.[10] It was found by EELS carried out by STEM that the center of oxide precipitates consists of SiO_2 surrounded by suboxides with decreasing x towards the edges. In Fig. 4, an example of such a stoichiometry profile across a plate-like oxide precipitate of 9.7 nm thickness is shown.[10] Its composition can be well explained by the modelling results.

It was also discovered recently that the suboxides are gettering sinks for Cu impurities.[14] Therefore, it would be interesting to understand how n_{crit} depends on parameters like annealing temperature and density of oxide precipitates. A further point of interest would be how the emission of self-interstitials depends on these parameters. In Fig. 5, the results of modeling are shown for different temperature and density of oxide precipitates. It can be seen that for any temperature both n_{crit} and maximum β decrease with increasing density of oxide precipitates. In addition to this, n_{crit} and maximum β increase with increasing temperature for any density of oxide precipitates. This means that the availability of suboxides for gettering of Cu impurities depends on both the annealing temperature and the density of oxide precipitates.

Figure 6 shows the maximum β as function of N for different temperatures. With decreasing temperature the emission of self-interstitials decreases. This is well in agreement with experimental results of Torigoe and Ono.[27] They used the enhancement of B-diffusion to estimate the emission of self-interstitials during anneals in the range from 850 °C to 1000 °C for up to 72 h assuming that β is constant for given anneal temperatures and independent of the density of oxide precipitates. According to our findings this should not be the case. Because of this, we can only compare the trends but cannot directly adjust our results to their experimental data. Sueoka et al. reported a similar trend, decreasing β with decreasing temperature, for his experimental results.[22]

In Fig. 7, we plotted the critical radius for formation of suboxides r_{crit} as function of the density of oxide precipitates for different annealing temperature. This critical radius is of significance for the ability of oxide precipitates to getter metallic impurities like Cu at all. Precipitates with a radius up to r_{crit} would consist of pure SiO_2 without any suboxide. It can be seen in Fig. 7 that with increasing

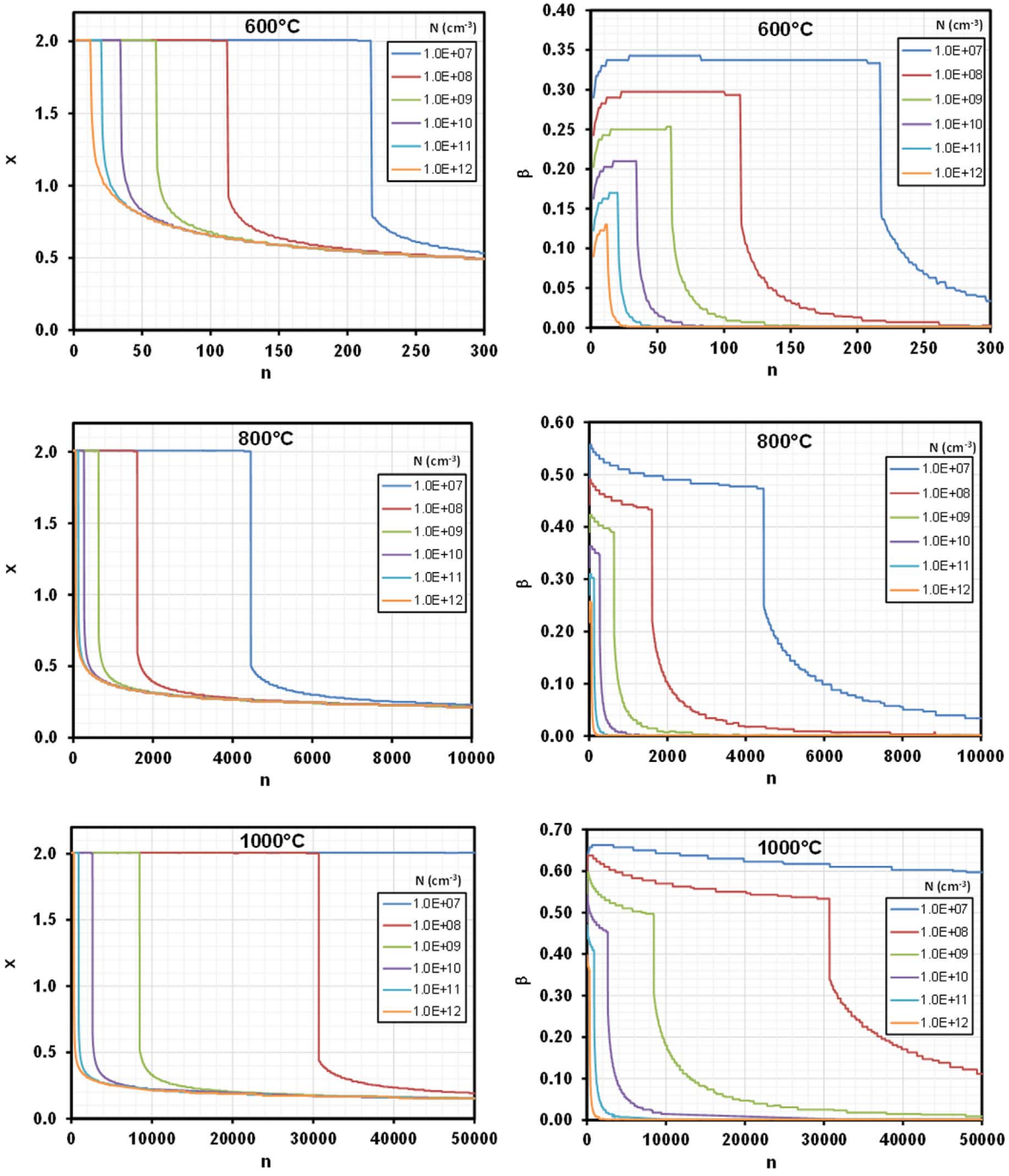

Figure 5. Left: stoichiometry of oxide precipitates x plotted as function of the number of oxygen atoms in the precipitate n shown for different densities of oxide precipitates N and different temperature. Right: self-interstitials emitted per precipitated oxygen atom β plotted as function of the number of oxygen atoms in the precipitate n shown for different densities of oxide precipitates N and different temperature. For modelling $C_{Oi}^{0} = 6 \times 10^{17}$ cm^{-3} was assumed.

density of oxide precipitates the critical radius decreases. It also decreases with decreasing temperature.

For efficient gettering of metallic impurities however, a certain amount of suboxide is needed. In the following, we estimate the amount of suboxide by calculating the number of oxygen atoms in suboxide assuming that the precipitate continues to grow as SiO_2 and neglecting inter-diffusion. The number of oxygen atoms in a precipitate after annealing for certain time at certain temperature can be calculated numerically using

$$\frac{\partial n}{\partial t} = n^{1/3} \cdot D_{Oi} \cdot [C_{Oi}(t) - C_{Oi}^{if}] \cdot \left(\frac{48\pi^2\Omega_P}{x}\right)^{1/3} \quad [13]$$

with D_{Oi} being the diffusion coefficient of interstitial oxygen taken from Ref. 21. Then, the number of oxygen atoms in suboxide n_{sub} is

$$n_{sub} = N \cdot [n(t) - n_{crit}]. \quad [14]$$

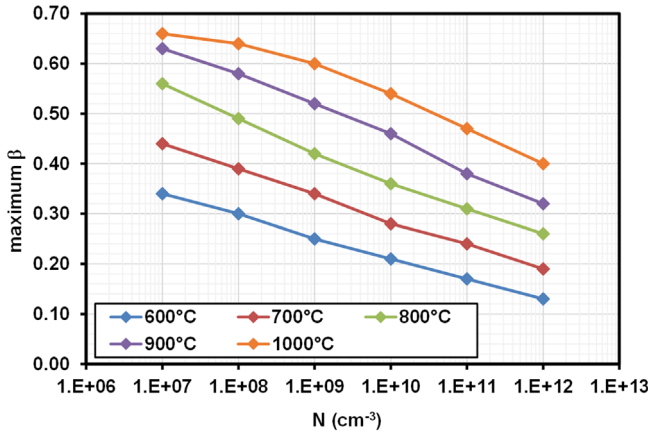

Figure 6. Maximum number of self-interstitials emitted per precipitated oxygen atom plotted as function of the density of oxide precipitates N shown for different temperatures. For modelling $C_{Oi}^{0} = 6 \times 10^{17}$ cm^{-3} was assumed.

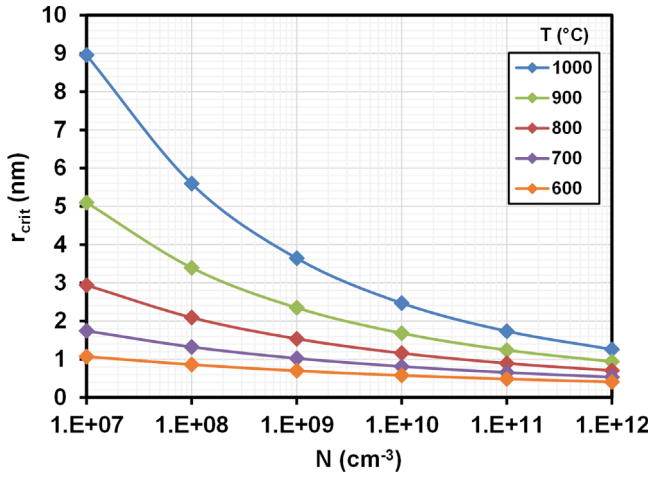

Figure 7. Critical radius for suboxide formation plotted as function of the density of oxide precipitates for different annealing temperatures. For modelling $C_{Oi}^{0} = 6.5 \times 10^{17}$ cm^{-3} was assumed.

We can define a getter efficiency η as follows

$$\eta = \begin{cases} 0\% & \text{for } n(t) < n_{crit} \\ \dfrac{n_{sub}}{n_{sub}^{crit}} & \\ 100\% & \text{for } n_{sub} > n_{sub}^{crit} \end{cases} \quad [15]$$

with n_{sub}^{crit} being the critical amount of oxygen atoms in suboxide needed to be able to getter 100% of Cu impurities.

In Fig. 8, the results of modeling the getter efficiency for annealing at 800 °C and 1000 °C are shown. It can be seen that the higher the density of oxide precipitates is the faster 100% getter efficiency is reached. For very high densities of oxide precipitates the time to achieve efficient gettering of oxide precipitates is extremely short. It increases markedly with decreasing density of oxide precipitates. This decrease is not linearly because r_{crit} and thus also n_{crit} are functions of the density of oxide precipitates as demonstrated in Fig. 7.

Modeling oblate spheroidal oxide precipitates.—The model for oblate spheroidal oxide precipitates was set up to get information about the precipitate morphology of lowest free energy in addition to the optimum β and x. Several authors used the minimized excess free energy being the sum of ΔG_{σ} and ΔG_{ε} to determine the aspect ratio γ.[22,27–29] However, all the models in these papers are based on

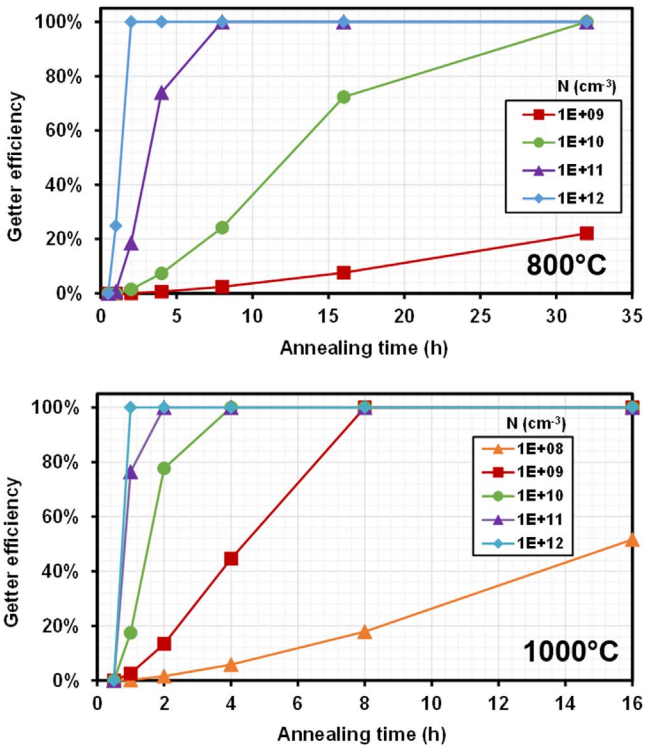

Figure 8. Getter efficiency as function of annealing time at 800 °C (above) and 1000 °C (below) shown for different density of oxide precipitates. For modelling $C_{Oi}^{0} = 6.5 \times 10^{17}$ cm^{-3} was assumed.

constant x and β. Therefore, it is interesting to investigate which composition, shape, and self-interstitial emissivity oxide precipitates would prefer in quasi-equilibrium. Because the emission of self-interstitials during precipitation depends on N and affects ΔG_v we do not reduce our model to just the excess free energy.

Figure 9 shows with some examples how β and γ would evolve in quasi-equilibrium as function of n for different density of oxide precipitates. The outcome of running our three-dimensional model was that in any case $\gamma = 0.999$, a sphere, is the energetically preferred geometry for low numbers of oxygen atoms in any precipitate in the investigated temperature range from 600 °C to 1100 °C. This is well in agreement with the results of Sueoka et al.[30] The preferred phase is always SiO_2 and the emission of self-interstitials is high. In Fig. 9, the evolution of x is not shown because it stays constantly at a value of about 2 even after β and γ exhibit a sudden drop at a critical number of oxygen atoms n_{crit}. This means that when n_{crit} is reached the precipitate changes its shape from sphere to platelet and stops the emission of self-interstitials maintaining a composition of SiO_2. The optimum aspect ratio of the platelets lies between 0.02 and 0.03. In Fig. 9, it can be seen that for any temperature in the investigated range both n_{crit} and maximum β decrease with increasing density of oxide precipitates. In addition to this, n_{crit} and maximum β increase with increasing temperature for any density of oxide precipitates.

Figure 10, the critical side length for morphology change of octahedral precipitates a_{crit} is plotted as function of the density of oxide precipitates for different annealing temperatures. We have chosen here the side length of octahedral precipitates with equivalent volume because in the next section we compare our modeling results with results of STEM investigations and spherical precipitates just represent the octahedral morphology which is observed experimentally. It can be seen in Fig. 10, that the critical size for morphology change depends on the density of oxide precipitates. At 1000 °C, this dependency is very distinct. The reason for this dependency of the critical size on the density of oxide precipitates is first of all the

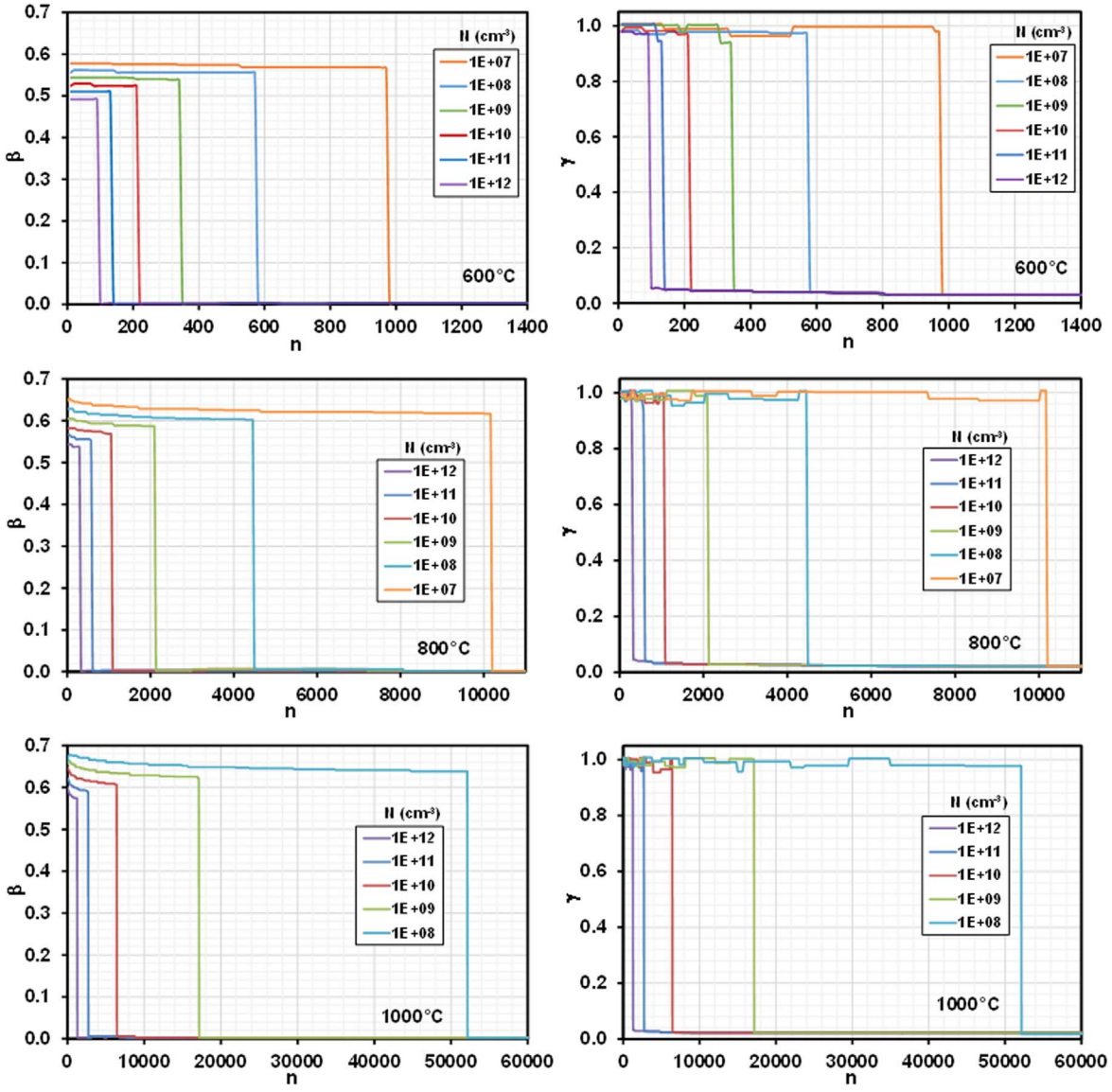

Figure 9. Left: self-interstitials emitted per precipitated oxygen atom β plotted as function of the number of oxygen atoms in the precipitate n shown for different densities of oxide precipitates N and different temperature. Right: aspect ratio γ plotted as function of the number of oxygen atoms in the precipitate n shown for different densities of oxide precipitates N and different temperature. For modelling $C_{Oi}^{0} = 6.5 \times 10^{17}\,\mathrm{cm}^{-3}$ was assumed.

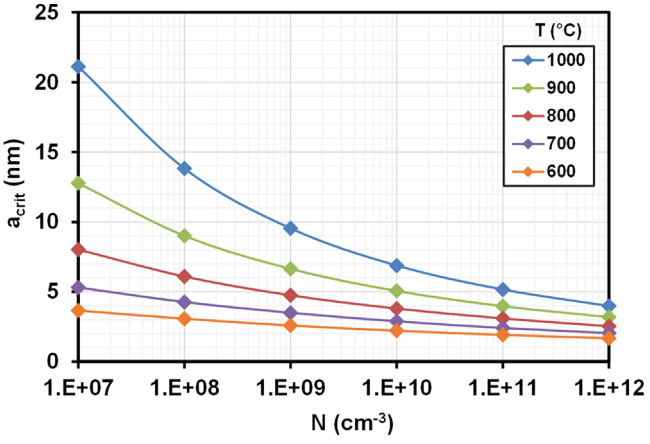

Figure 10. Critical side length for morphology change of octahedral precipitates plotted as function of the density of oxide precipitates for different annealing temperatures. For modelling $C_{Oi}^{0} = 6.5 \times 10^{17}\,\mathrm{cm}^{-3}$ was assumed.

higher concentration of self-interstitials generated by a higher density of oxide precipitates.

During annealing of silicon wafers, self-interstitials can diffuse to the wafer surface and recombine. The impact of this out-diffusion effect on the critical size was included into the model via the factor F which simply reduces the density of emitted self-interstitials assuming a certain amount left the system by out-diffusion. In Fig. 11, an example with $N = 10^{10}\,\mathrm{cm}^{-3}$ oxide precipitates is demonstrating that out-diffusion would increase a_{crit}. The increase with decreasing F follows a power law. This means that below the surface of silicon wafers the morphology change is expected to occur later than in the bulk. This is in agreement with the results of Fujimori[23] who found octahedral oxide precipitates mainly below the surface.

Our model considerations refer to equilibrium conditions and in reality it is not possible that an octahedral precipitate can just simply switch into a platelet. However, the octahedral morphology is not stable anymore after the critical size is reached. In the next section, we compare the modeling results with morphology investigations by STEM.

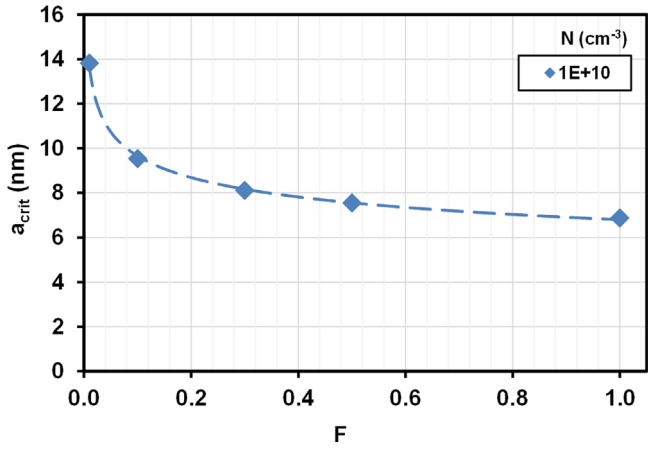

Figure 11. Critical side length for morphology change of octahedral precipitates plotted as function of F respecting the out-diffusion of emitted self-interstitials. For modelling $C_{Oi}^{0} = 6.5 \times 10^{17}\,\mathrm{cm}^{-3}$ and $N = 10^{10}\,\mathrm{cm}^{-3}$ were assumed.

Comparison of Modeling with Experimental Results and Discussion

Evolution of oxide precipitate morphology.—We investigated samples of silicon wafers annealed at 1000 °C for times up to 30 h by STEM with a density of oxide precipitates of about $1 \times 10^{10}\,\mathrm{cm}^{-3}$. Octahedral oxide precipitates could be observed only below the surface of the silicon wafers up to a depth of 100 μm or less depending on the annealing time. With further increasing depth we first detected transition forms between octahedral and platelets and then only platelets. With increasing annealing time the depth up to which octahedral precipitates were observed decreased. This is well in agreement with the results of modeling oblate spheroidal oxide precipitates. Below the surface, part of the emitted self-interstitials can diffuse out and the increased a_{crit} makes the octahedral morphology more stable for higher n. When the octahedral morphology becomes unstable, what happens first in the bulk, the precipitates start changing their morphology as demonstrated in Fig. 12. Figure 12a shows an octahedral precipitate below the surface before the morphological transition starts. It can be seen in Fig. 12b that growth in [111] direction is retarded and growth in [110] directions around the edges of the octahedron is enhanced. In Fig. 12c, this is further proceeded and a platelet evolving from the octahedron becomes visible. Fig. 12d shows a large platelet with the original octahedron and in Fig. 12e only the platelet is existing anymore. Via surface reconstruction the atoms of the original octahedron distribute on the (100) surface of the platelet. This can also lead to structures of dendritic precipitates as reported by Aoki[30] and in Ref. 31.

The evolution of the morphology of growing oxide precipitates which we observed by depth dependent STEM studies of precipitate morphologies at different annealing times is well in agreement with results of modeling. However, it is exactly the opposite to the evolution model of Bergholz et al.[32] They investigated oxide precipitates in silicon annealed for times from 48 h to 431 h at 750 °C by TEM. They found morphologies similar to Fig. 12d. Looking at such image it tempts you to assume that first there was a platelet and the fins evolve in the second step. It should be mentioned here also that the morphology evolution model of Bergholz et al. is the basis of the theory of the so-called "ninja" plates.[1]

Gettering of copper impurities.—The question that arises when the outcome of the spherical and oblate spheroidal model are compared is: Can suboxides be formed at all because a morphology change from sphere to platelet is the preferred way to reduce the free energy? The problem is the kinetics of a morphology change, it proceeds much more slowly than a change of stoichiometry. So when a_{crit} is reached both processes can be expected to start, morphology change as well as stoichiometry change, because the SiO_2 precipitates with octahedral morphology become unstable and the system wants to lower its free energy. Both processes are accompanied by a drop of the emission of self-interstitials. Therefore, we continue to explore the outcome of the spherical model for its relevance to explain gettering of copper impurities.

We can distinguish three different states of oxide precipitates being relevant for gettering. If their size is subcritical they are unable to getter copper impurities. They consist of SiO_2 at this stage. When the number of precipitated oxygen atoms exceeds the critical number gettering becomes possible but the efficiency is not high enough to getter all of the metal atoms. If the oxygen atoms in the suboxide exceed a critical number the precipitates can efficiently getter the copper impurities. It was demonstrated in Fig. 8 that the time to reach efficient gettering strongly depends on the density of oxide precipitates. This is well in agreement with Ref. 1 but based on an alternative explanation for the effects described there.

In the following, we compare the results of our copper getter tests with modeled thresholds for efficient gettering. The lower graphs in Fig. 13 show the densities of oxide precipitates detected by preferential etching in the samples of wafers pre-treated by RTA and subsequently annealed at 800 °C for different times. The RTA temperature defines the density of oxide precipitate nuclei in the samples.[33,34] During annealing at 800 °C they grow but if they are not large enough to survive the fast ramp to the 1000 °C growth anneal they will not become detectable by preferential etching. For this reason, the oxide precipitate density first increases with increasing annealing time at 800 °C until a saturation level is reached. The density at the saturation level is the density of oxide precipitate nuclei installed by RTA. The annealing time at 800 °C defines the size of the oxide precipitates. The wafers co-doped with nitrogen (left graph) contain a somewhat higher density of oxide precipitates because nitrogen enhances oxide precipitation.[35,36]

The upper graphs in Fig. 13 provide the corresponding measured getter efficiencies for copper. In both graphs an unexpected effect can be observed. For short annealing times a getter efficiency of up to 80% exists which rapidly drops down before it increases again in most cases for annealing times larger than 4 h. Until now, such effects were only observed for silicon wafers with very low oxygen concentration.[37] In wafers with very low oxygen concentration tiny vacancy clusters can be formed during high temperature RTA.[20] These are able to getter Ni and Cu immediately after RTA but they are not stable and the getter effect is lost by further annealing at $T \geqslant 800$ °C.[37] Modelling of the formation and dissolution of vacancy clusters is well in agreement with these observations.[38] For wafers with high oxygen concentration, the effect of nano-void formation is not expected because it is assumed that the vacancies bind to oxygen. Experiments with haze tests confirmed this.[37] In the getter tests of this work, the contamination level is markedly lower than during haze tests, and a getter effect of nano-voids is detectable for both concentrations of interstitial oxygen being high and medium. This would mean that even for medium and high concentrations of interstitial oxygen vacancy agglomeration would be possible. We do not follow up this topic here further because it is not in the focus of this article. For the comparison with our modeling results, we use only the getter efficiencies for times larger than 4 h of annealing at 800 °C because these are caused by oxide precipitates. Looking at the results in Fig. 13, it can be seen that for high N a high getter efficiency is reached after relatively short annealing time at 800 °C but for low N even 32 h are not sufficient to reach getter efficiencies $\geqslant$90%. This is well in agreement with the theoretical results of Fig. 8 (above).

In Fig. 14 above and below, the getter efficiencies of experimental samples are compared with modelled getter efficiencies, respectively. For this purpose, the getter efficiencies of the samples annealed for different times at 800 °C were plotted as function of radius and density of oxide precipitates. The correlation between experimental and theoretical results is very good and the threshold

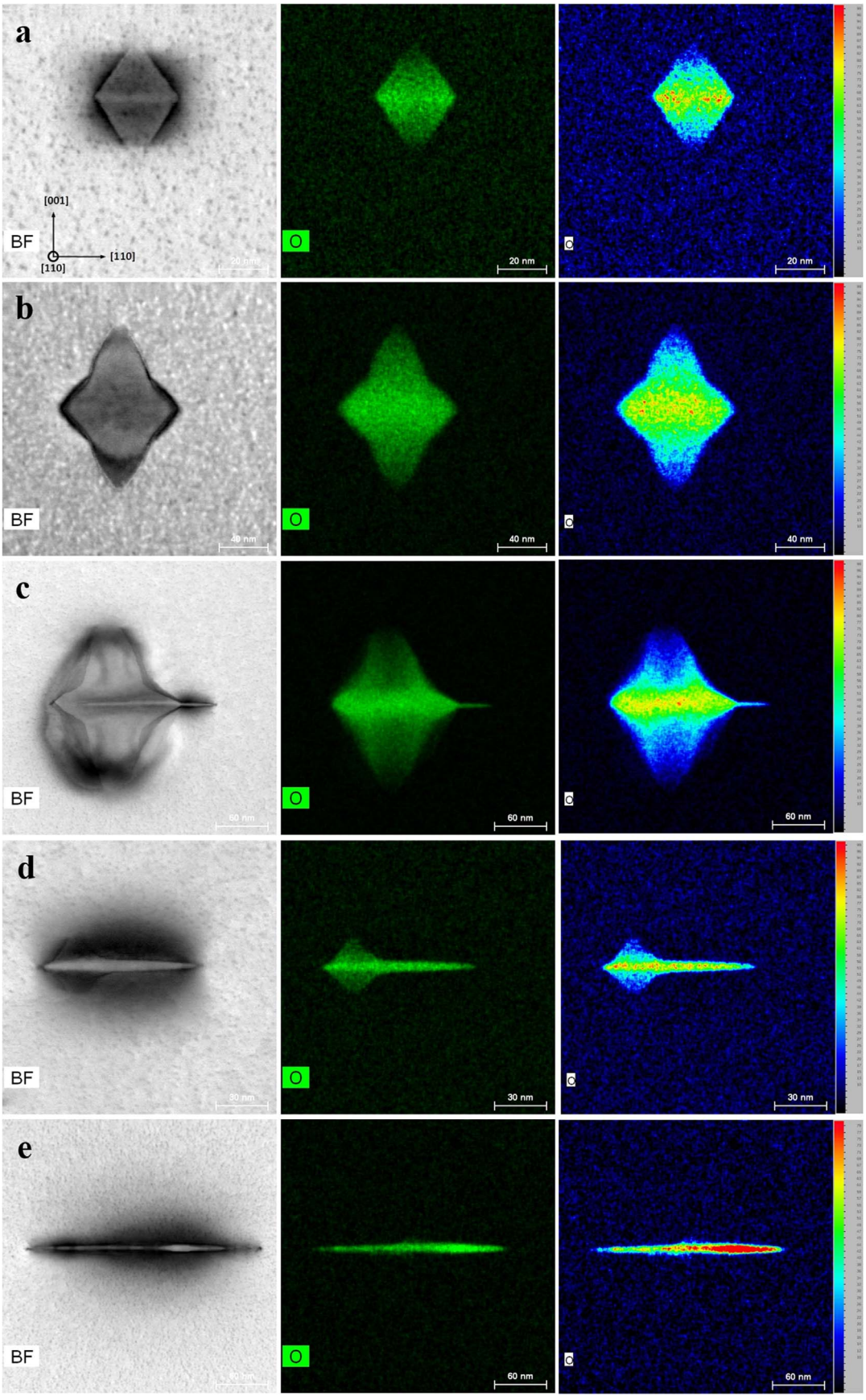

Figure 12. TEM images of oxide precipitates annealed at 1000 °C reflecting the evolution of precipitate morphology from top to bottom. Left column: STEM bright field images (dark contrasts are caused by strain fields), middle column: EDX maps of oxygen, and right column: mapping of oxygen counts in arbitrary units increasing from blue to red.

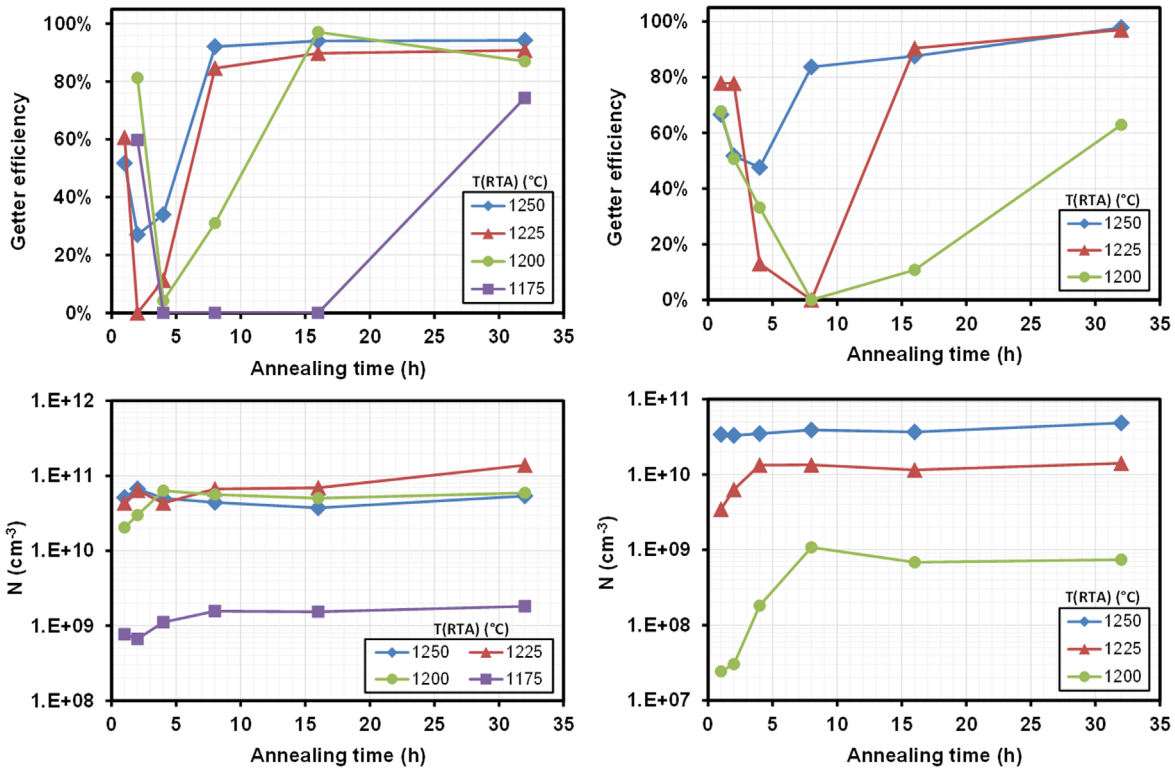

Figure 13. Above: Getter efficiency for Cu plotted as function of the annealing time at 800 °C for wafers pre-treated by RTA at different temperature. Below: Oxide precipitate density plotted as function of the annealing time at 800 °C for wafers pre-treated by RTA at different temperature. Left and right graphs belong to wafers with $C_{Oi}^{0} = 6.5 \times 10^{17}\,\mathrm{cm}^{-3}$ and $C_{Oi}^{0} = 8.5 \times 10^{17}\,\mathrm{cm}^{-3}$, respectively.

for efficient gettering is the same. The threshold for efficient gettering would be $1.2 \times 10^{13}\,\mathrm{cm}^{-2}$. This holds for 200 mm wafers. This number of oxygen atoms in the suboxide per cm^2 is comparable to the maximum contamination level in the getter tests.

The results of the getter tests carried out after growth anneal at 1000 °C for 16 h are compared in Fig. 15 with the theoretical values from modelling. The theoretical and experimental results are also quite well in agreement. Here a threshold for efficient gettering of $9.1 \times 10^{13}\,\mathrm{cm}^{-2}$ was found which is different from the threshold value at 800 °C. This is reasonable because it is segregation gettering and the segregation coefficient depends on the temperature.

Lifetime of minority carriers.—It should be further explored if the decrease in the lifetime of minority carriers could be caused by suboxide formation. Danilov et al. investigated annealed silicon samples by TEM and space charge spectroscopy and concluded that the charge accumulation is localized in the suboxide region of oxide precipitates due to broken SiO_x bonds, whereas the SiO_2 core remains electrically neutral.[39] Lang et al. found by electrically detected magnetic resonance that photo-excited electron-hole pairs recombine through dangling bonds of P_{b0} and P_{b1} type at oxide precipitates.[16] Murphy et al. carefully investigated the lifetime degradation effects of oxide precipitates.[8] They excluded other factors contributing to lifetime from the measurement results and isolated the contribution from oxide precipitates and their secondary defects. They found that at so-called unstrained "ninja" precipitates the recombination is weak and correspondingly the lifetime is very high. According to our theoretical results these could be the pure spherical or better octahedral SiO_2 precipitates which can be expected to form in the initial stages of oxide precipitation because their free energy is the lowest. Murphy et al. also found that recombination at so-called strained precipitates is much stronger and depends on the density of precipitates rather than on their size.[8] In a later work, Murphy et al. concluded that the density of recombination centers associated with oxide precipitates more likely depends on their interface area.[10] Generally spoken, it seems that the recombination activity of oxide precipitates behaves similar to the suboxide formation.

Murphy et al. used silicon samples with different nucleation time at 650 °C (6 h, 8 h, 16 h, and 32 h) to generate different densities of oxide precipitates, stabilized them at 800 °C for 4 h followed by different times of growth annealing at 1000 °C (0.5 h, 1 h, 2 h, 4 h, 8 h, and 16 h) to get different sizes of oxide precipitates.[8] We used these thermal conditions and determined the density of oxygen atoms precipitating in suboxides. We plotted these as a function of the time of growth annealing at 1000 °C for different densities of oxide precipitates in Fig. 16 (above). It can be seen that it is not possible to correlate the density of oxygen atoms in the suboxide directly to the annealing time for any density of oxide precipitates. The correlation is linear but with different slope for the different densities of oxide precipitates. The reason for this was demonstrated in the beginning of this article. The critical size for the onset of suboxide formation strongly depends on the density of oxide precipitates (please see Fig. 7). It can be also seen in Fig. 16 (above) that for very short times of growth annealing $\leqslant$ 1 h no suboxide exists. This is well in agreement with the appearance of only "unstrained precipitates" in Ref. 7. In Fig. 16 (below), we plotted the lifetime data of Murphy et al.[8] as reciprocal lifetime vs the time of growth annealing for different times of nucleation annealing. The time of nucleation annealing determines the density of oxide precipitates ranging from a few $10^6\,\mathrm{cm}^{-3}$ to $10^{11}\,\mathrm{cm}^{-3}$ in Ref. 8. Both graphs, Fig. 16 above and below, exhibit similar behavior meaning that the recombination activity of oxide precipitates indeed could correlate with suboxide formation.

A process with very high probability affected by the charges in the suboxide is preferential etching of oxide precipitates. This could explain why subcritical oxide precipitates cannot be detected by preferential etching because they consist of uncharged SiO_2.[39]

Information about the strain of the oxide precipitates can be obtained from the bright field STEM images in Fig. 12 (left side)

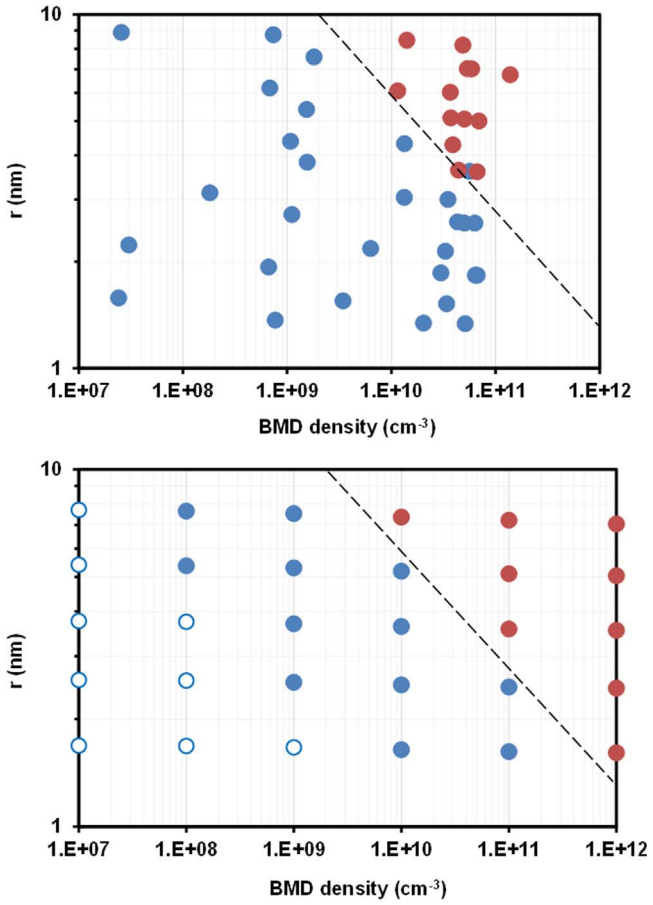

Figure 14. Getter efficiency of samples annealed for different times at 800 °C plotted as function of radius and density of oxide precipitates, above: experimental values from Cu getter tests, below: theoretical values. Full red circles represent high getter efficiencies ⩾90%, full blue circles represent inefficient gettering, and empty blue circles represent precipitates theoretically being unable to getter at all.

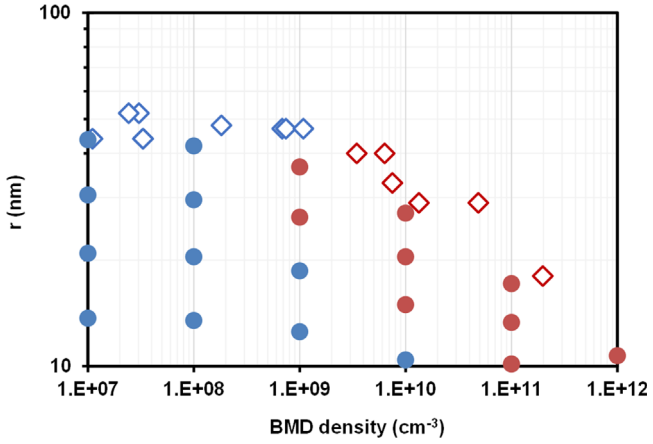

Figure 15. Getter efficiency of samples annealed for different times at 1000 °C plotted as function of radius and density of oxide precipitates. Red symbols represent high getter efficiencies ⩾90%, blue symbols represent inefficient gettering, empty diamonds stand for experimental values from Cu getter tests and full spheres stand for theoretical values.

where it becomes visible in as a dark contrast around the oxide precipitates. All precipitates, except 12b where it is very weak, exhibit a clear strain contrast. However, a darker contrast does not automatically mean that the strain is larger. Quantification of strain in TEM needs very sophisticated efforts. It can be carried out by

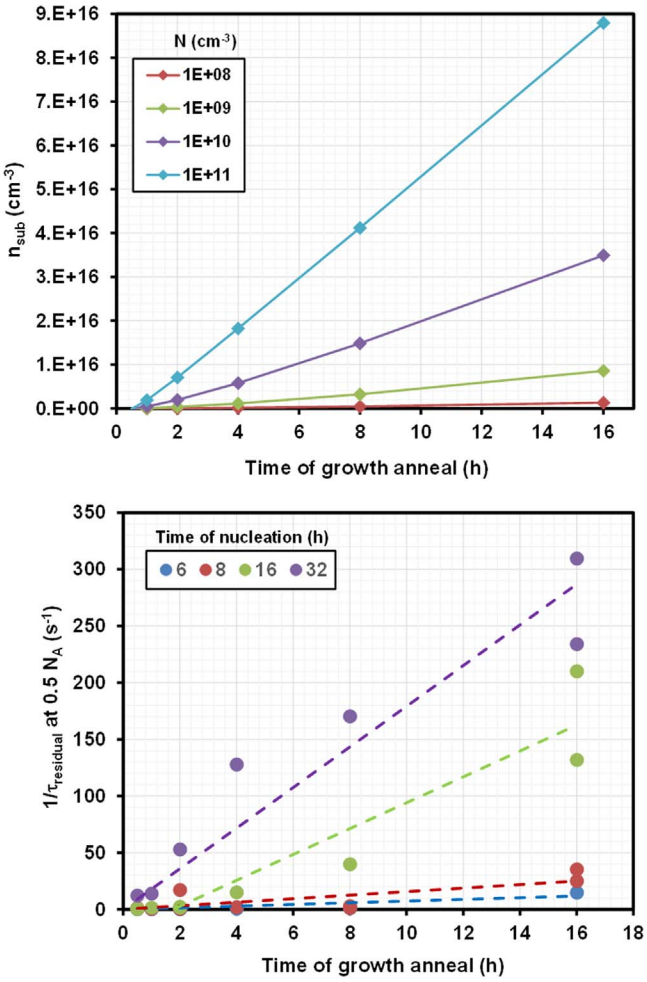

Figure 16. Above: number of oxygen atoms in suboxide plotted as function of the annealing time at 1000 °C for different density of oxide precipitates. Below: Residual lifetime values published by Murphy et al.[8] measured at 0.5 N_A (doping level) plotted here as reciprocal values against the time of growth annealing at 1000 °C for different times of nucleation annealing at 650 °C.

convergent beam electron diffraction (CBED).[40] The only conclusion from Fig. 12 that can be drawn concerning strain is that all precipitates observed, small octahedral as well as transitional morphologies and platelets are strained. Yonemura et al. carried out CBED measurements of the strain field around oxide precipitates of different morphology. They found that the strain field, decreasing monotonically as a function of the distance from the precipitate/matrix interface, is controlled by the size, morphology and local shape of the precipitate.[40]

Conclusions

The aim of this work was to find out the optimum path of growing oxide precipitates with respect to their stoichiometry, emission of self-interstitials and morphology. This was done by minimizing the free energy based on classical nucleation theory. The comparison with experimental results from ourselves and from the literature allowed us to understand the important role of suboxides for internal gettering of copper impurities and for carrier recombination at oxide precipitates being important for lifetime control. Comparison with experimental results allowed us to deduce the sequence of morphology evolution of oxide precipitates. In the following, we summarize the most important conclusions from this work.

Applying the model for spherical oxide precipitates, it was found that for low numbers of precipitating oxygen atoms the composition

is SiO_2 and the self-interstitial emission relieving the strain is very high. With increasing n, the emission of self-interstitials slightly decreases up to a critical number of precipitated oxygen atoms n_{crit}. Then, the minimum free energy suddenly jumps to low values of x, changing the stoichiometry into a suboxide, accompanied by very low emission of self-interstitials. The critical number of precipitated oxygen atoms decreases with increasing density of oxide precipitates and it increases with increasing temperature. This means that the availability of suboxides for gettering of Cu impurities depends on both the annealing temperature and the density of oxide precipitates. For very high densities of oxide precipitates the time to achieve efficient gettering of oxide precipitates is extremely short. It increases markedly with decreasing density of oxide precipitates.

Applying the model for oblate spheroidal precipitates similarly to the model for spherical precipitates for low numbers of precipitating oxygen atoms the composition is SiO_2 and the self-interstitial emission relieving the strain is very high. For low numbers of precipitating oxygen atoms, the morphology is also spherical. However, when n_{crit} is reached the precipitate changes its shape from sphere to platelet and stops the emission of self-interstitials maintaining a composition of SiO_2. The optimum aspect ratio of the platelets lies between 0.02 and 0.03.

The modeling results refer to homogeneous oxide precipitates under quasi-equilibrium conditions. In reality, the kinetics of morphology change is much more slowly than a change of stoichiometry, which just happens during the attachment of new atoms. Therefore, when the octahedral morphology gets unstable suboxides can be expected to form as well. The stages of morphology change start at octahedral morphology. Then the growth into ⟨110⟩ directions starting at the edges of the octahedron is enhanced until a platelet evolves from the octahedron and the original octahedron remains as fins on the platelet before it vanishes completely. The rate of morphology change depends on the possibility of out-diffusion of the generated self-interstitials and thus on the depth from the wafer surface.

The formation of suboxides at the edges of oxide precipitates after reaching a critical size is reached can explain several phenomena like gettering of Cu by segregation to the suboxide region and lifetime reduction by recombination of minority carriers in the suboxide. It thus provides an alternative explanation, based on minimized free energy, to the theory of strained and unstrained plates.

Acknowledgments

The first author would like to thank Dr. J. W. P. Schmelzer from University of Rostock for the inspiring discussion.

ORCID

G. Kissinger https://orcid.org/0000-0002-6492-3117

References

1. R. Falster, V. V. Voronkov, V. Y. Resnik, and M. G. Milvidskii, "Proc. electrochem. soc., high purity silicon VIII." *High Purity Silicon VIII* (The Electrochem. Soc., Pennington, NJ, USA) Vol. 2004–05, p. 188 (2004).
2. V. V. Voronkov, R. Falster, T. H. Kim, S. S. Park, and T. Torack, *J. Appl. Phys.*, **114**, 043520 (2013).
3. G. Kissinger, J. Dabrowski, A. Sattler, T. Müller, and W. von Ammon, *Solid State Phenom.*, **131–133**, 293 (2008).
4. G. Kissinger and J. Dabrowski, *J. Electrochem. Soc.*, **155**, H448 (2008).
5. G. Kissinger, J. Dabrowski, A. Sattler, C. Seuring, T. Müller, H. Richter, and W. von Ammon, *J. Electrochem. Soc.*, **154**, H454 (2007).
6. D. Kot, G. Kissinger, M. A. Schubert, S. Marschmeyer, G. Schwalb, and A. Sattler, *Phys. Stat. Sol. (c)*, **14**, 1700161 (2017).
7. K. Bothe, R. J. Falster, and J. D. Murphy, *Appl. Phys. Lett.*, **101**, 032107 (2012).
8. J. D. Murphy, K. Bothe, M. Olmo, V. V. Voronkov, and R. J. Falster, *J. Appl. Phys.*, **110**, 053713 (2011).
9. G. Kissinger, J. Vanhellemont, E. Simoen, C. Claeys, and H. Richter, *Mat. Sci. Eng. B*, **36**, 225 (1996).
10. J. D. Murphy, M. Al-Amin, K. Bothe, M. Olmo, V. V. Voronkov, and J. R. Falster, *J. Appl. Phys.*, **118**, 215706 (2015).
11. G. Kissinger, M. A. Schubert, D. Kot, and T. Grabolla, *ECS J. Solid State Sci. Technol.*, **6**, N54 (2017).
12. J. Vanhellemont, *Phys. Status Solidi RRL*, **1–5**, 597 (2015).
13. E. Kamiyama and K. Sueoka, *ECS J. Solid State Sci. Technol.*, **7**, P102 (2018).
14. G. Kissinger, D. Kot, M. Klingsporn, M. A. Schubert, A. Sattler, and T. Müller, *ECS J. Solid State Sci. Technol.*, **4**, N124 (2015).
15. J. D. Murphy, K. Bothe, V. V. Voronkov, and R. Falster, *Appl. Phys. Lett.*, **102**, 042105 (2013).
16. V. Lang, J. D. Murphy, R. J. Falster, and J. J. L. Morton, *J. Appl. Phys.*, **111**, 013710 (2012).
17. J. Vanhellemont, *J. Appl. Phys.*, **78**, 4297 (1995).
18. F. R. N. Nabarro and H. H. Wills, *Proc. Roy. Soc., A*, **175**, 519 (1940).
19. H. Takeno, Y. Hayamizu, and K. Miki, *J. Appl. Phys.*, **84**, 3113 (1998).
20. T. A. Frewen and T. Sinno, *Appl. Phys. Lett.*, **89**, 191903 (2006).
21. J. C. Mikkelsen Jr, *Mater. Res. Soc. Symp. Proc.*, **59**, 19 (1986).
22. K. Sueoka, N. Ikeda, T. Yamamoto, and S. Kobayashi, *J. Appl. Phys.*, **74**, 5437 (1993).
23. H. Fujimori, *J. Electrochem. Soc.*, **144**, 3180 (1997).
24. D. Kot, G. Kissinger, M. A. Schubert, and A. Sattler, *ECS J. Solid State Sci. Technol.*, **3**, P370 (2014).
25. F. Secco d'Aragona, *J. Electrochem. Soc.*, **199**, 948 (1972).
26. D. Kot, G. Kissinger, A. Sattler, and T. Müller, *Acta Phys. Pol. A*, **125**, 965 (2014).
27. K. Torigoe and T. Ono, *J. Appl. Phys.*, **121**, 215103 (2017).
28. K. Sueoka, M. Akatsuka, M. Okui, and H. Katahama, *J. Electrochem. Soc.*, **150**, G469 (2003).
29. Y. Yang, A. Sattler, and T. Sinno, *J. Appl. Phys.*, **125**, 165705 (2019).
30. S. Aoki, *Mater. Trans.*, **34**, 746 (1993).
31. D. Kot, G. Kissinger, M. A. Schubert, and A. Sattler, *Appl. Phys. Lett.*, **104**, 182101 (2014).
32. W. Bergholz, M. J. Binns, G. R. Booker, J. C. Hutchison, S. H. Kinder, S. Messoloras, R. C. Newman, R. J. Stewart, and J. G. Wilkes, *Phil. Mag. B*, **59**, 499 (1989).
33. R. Falster, M. Pagani, D. Gambaro, M. Cornara, M. Olmo, G. Ferrero, P. Pichler, and M. Jacob, *Solid State Phenom.*, **57–58**, 129 (1997).
34. G. Kissinger, "Oxygen precipitation in silicon." *Defects and Impurities in Silicon Materials*, ed. Y. Yoshida and G. Langouche (Springer, Japan) p. 273 (2015).
35. D. Yang and X. Yu, *Solid State Phenom.*, **230–232**, 199 (2004).
36. G. Kissinger, G. Raming, R. Wahlich, and T. Müller, *Physica B*, **407**, 2993 (2012).
37. G. Kissinger, D. Kot, and W. Häckl, *ECS Trans.*, **33**, 113 (2010).
38. G. Kissinger, J. Dabrowski, T. Sinno, Y. Yang, D. Kot, and A. Sattler, *J. Cryst. Growth*, **468**, 424 (2017).
39. D. Danilov, O. Vyvenko, A. Loshachenko, and N. Sobolev, *Phys. Stat. Sol. (a)*, **216**, 1900327 (2019).
40. M. Yonemura, K. Sueoka, and K. Kamei, *Jpn. J. Appl. Phys.*, **38**, 3440 (1999).